SINET: Ethiop. J. Sci., 38(2):111-126, 2015 ISSN: 0379–2897 (Print)
 2520–7997 (Online)

GEOLOGY AND GEOCHRONOLOGY OF THE MUSH PALEONTOLOGICAL SITE, NORTH-CENTRAL ETHIOPIA

Mulugeta Feseha

Paleoanthropology and Paleoenvironment Program, College of Natural Sciences, Addis Ababa University, Addis Ababa, Ethiopia. E-mail: mulugetafyg@gmail.com; mulugeta.feseha@aau.edu.et

ABSTRACT: The Mush basin, located in north central Ethiopia, has yielded a 21.736 Ma floral and faunal assemblages, with significant potential for paleoclimate reconstruction and new data on the geological history of the Ethiopian Highlands. It lies in a volcanic province typified by thick successions of Tertiary volcanics and interbeded lacustrine sequences. Research was conducted in the Mush basin with multiple objectives including: to document the origin, age, volcanic episodes, and overall evolution of the sedimentary basin; and to provide a physical setting for associated fossil flora, fauna, and paleoecological interpretations. Field survey, petrographic and XRD analyses, and radioisotopic age determinations were conducted to understand the geological history and environment of the sedimentary basin. The Mush lacustrine carbonaceous shales host abundant compressions of leaves, fruits, seeds, insects, concentrations of organically preserved amphibians, pollen, woods and remains of mammals. Fieldwork also identified nearby multiple volcanic episodes associated with volcanic bombs of up to a meter in diameter, and several *in situ* carbonized trees. The origin of the Mush basin is interpreted as volcanic caldera; and the early stage of lacustrine deposition is dated at 21.736±0.015Ma. X-ray diffraction analyses (which document the presence of kaolinite) and the study of field relationships indicate that the fossiliferous shales originated in a fresh water lake, which most likely formed in a volcanic caldera, and which had anoxic or hypoxic conditions at depth. These conclusions are consistent with the presence of organically-preserved amphibians and aquatic plants, and indicate a climate having abundant precipitation.

Keywords/phrases: Ethiopia, Lacustrine, Mush, Paleoclimate, Paleolake

INTRODUCTION

As has been well documented, during the Tertiary the northeastern part of Ethiopia was affected by the Arabia-Ethiopian swell caused by mantle pluming (Mohr, 1971; Berberi *et al*., 1972; Burke and Dewey, 1973; Dereje Ayalew *et al*., 2002, Dereje Ayalew, 2011), which generated volcanism resulting in massive flood basalts estimated to occupy a volume of about 350,000 km^3 over an area of about 600,000 km^2 (Mohr, 1983; Dereje Ayalew *et al*., 2002; Kieffer *et al*., 2004). Associated with this volcanism was the formation of several structural features such as half grabens, sags, depressions and full grabens which provided accommodation space for the formation of lacustrine and fluviatile sediments now exposed in different parts of the country. These ancient sedimentary sequences, or natural archives, produce evidence of ancient climate, fauna, flora and the geologic processes that formed them (e.g., Kappelman *et al*., 2003; Jacobs B., 2007; Garcia *et al*., 2010; Pan *et al*., 2010; Currano *et al*., 2011; Pan *et al*., 2012). As such, understanding these Tertiary sediments and the associated geologic processes of their formation results in an understanding of the landscape setting for ancient biota which is necessary for the understanding of Ethiopia's ancient ecosystems.

The interest of the author lies in pursuing Oligocene to Miocene environmental reconstructions in the broader context of development of a Eurasian - African land bridge, and concomitant global climate change. Faunal exchanges are known to have taken place during this time interval, but details of the process, the physical setting, and aspects of the associated climate and flora of the region continue to be documented. Research began with the depositional basins of Chilga Woreda in the North Gonder Zone of Amhara National Regional State in northwest Ethiopia, and this provided a record of 27-28 million year-old geology, fauna, flora, and climatic conditions (Mulugeta Feseha *et al*., 2001; Mulugeta Feseha, 2002; Kappelman *et al*., 2003; Mulugeta Feseha, 2005; García *et al*., 2006; Pan *et al*., 2006; Jacobs, B., 2007; Pan, A., 2007; Mulugeta Feseha, *et*

al., 2008; García *et al*., 2010; Jacobs, *et al*., 2010; Pan, A., 2010 and Pan, *et al*., 2010; Engel *et al*., 2013). More recently, research on the Mush locality of the North Shewa Zone of Amhara National Regional State in north-central Ethiopia has yielded the discovery of 21.736 million year-old fossil amphibians, fish, mammals, insects, and thousands of fossil plants (Mulugeta Feseha *et al*., 2008; Pan *et al*., 2012; Engel *et al*., 2013; Clemens, 2014). The main objectives of this paper is to present results and interpretations regarding the origin, age, and depositional environments of the Mush basin using XRD analysis, petrographic analysis, and radiometric age determinations. The research output will be a basis for the study of the Mush biota (through taxonomy and systematics as well as paleoecology), and the paleoclimate through the study of fossils, paleosols, and isotopes.

REGIONAL GEOLOGY

The Mush sedimentary deposits are located between 9°462453 to 9°47214.73 N and 39°382463 to 39°39230.53 E (157 km northeast of Addis Ababa) in North Shewa Zone of Amhara National Regional State in Ethiopia (Fig. 1). They harbor pre- Main Ethiopian Rift fauna and flora (Fig. 2), a record of geological processes, and information regarding paleoclimate and landscape. The depositional basin into which sedimentation took place, was a product of Neogene volcanism.

The study area is part of the central Ethiopian highlands and the western margin of the Main Ethiopian Rift and it consists of outcrops which include volcanics and associated coal-bearing sediments, originally explored for their economic potential by The Coal and Oil Shale Exploration Division and Regional Geology and Geochemistry Department of the Geological Survey of Ethiopia (Alula Habtegiorgis and Gashawbeza Mengstu, 1993; Gashawbeza Mengstuand Mesfin Wubshet, 1996; Yonas Hagereselam and Matebie Meten, 2006). These researchers have suggested that exposed pre-Miocene rocks appear to be uncommon in the studied region. The local geology, therefore, contains the oldest Alaji basalt (early Miocene) overlain by fluvial and lacustrine sediments (early Miocene), which in turn are overlain by rhyolite and ignimbrite units (early Miocene), capped by the Tarmaber basalt (late Miocene) Formation. Yonas Hagereselam and Matebie Meten (2006) have mapped the details of the Debrebirhan and Sela Dengay area, which is near the study area that is the subject of this paper. They distinguished a lower Basalt Unit (equivalent to the Alaji Basalt), a coal-bearing Sedimentary Unit, a Rhyolite and Ignimbrite Unit, and Upper Basalt Unit (equivalent to the Tarmaber basalt), from bottom to top. The lower basalt is exposed in highly dissected valleys and its lower contact is not exposed. This unit comprises strongly friable, fractured and jointed, dark grey, commonly aphanitic to locally phyric basalt. Overlying the lower basalt are the coal bearing sediments and ignimbrite units, which according to Yonas Hagereselam and Matebie Meten (2006) include two cycles of sedimentation separated by rhyolite and ignimbrite units. As reported by Alula Habtegiorgis and Gashawbeza Mengstu (1993) the total exposed thickness of the section is 27 meters, running along the flank of the Mush River and its nearby tributaries. Reworked tuffaceous sediments and carbonaceous shales intercalated with mudstones are observed interbedded with the coal seams. The rhyolites overlying these sediments are light grey to light bluish grey and fine to medium-grained in texture. In most cases, the rhyolites show clear stratification and locally contain rock fragments and collapsed pumice fiamme. The capping basalt actually consists of a number of flows separated by 0.25-0.4m thick paleosol layers. The basalts are olivine-plagioclase phyric, with minor intercalations of aphanitic, plagioclase porphiritic, olivine-phyric and pyroxene phyric compositions. This unit is affected tectonically by NNE-SSW trending faults running from Ankober to Tarmaber, which resulted in part of it having been down-thrown to the east (to Afar direction) (Alula Habtegiorgis and Gashawbeza Mengstu, 1993).

RESEARCH METHODS

The Mush basin was delineated in the field using GPS, and sedimentary exposures were located and mapped with the aid of thematic imagery and topographic maps. Sections were measured and described from exposures along the Mush River at which time samples were collected for petrographic analysis, radiometric dating and x-ray diffraction analyses. Stratigraphic sections were measured and described using a metered stick, Munsell soil color chart, and standard grain scale. Carbonaceous shales, volcanic ashes and lignite horizons served as markers to establish field relationships and correlations.

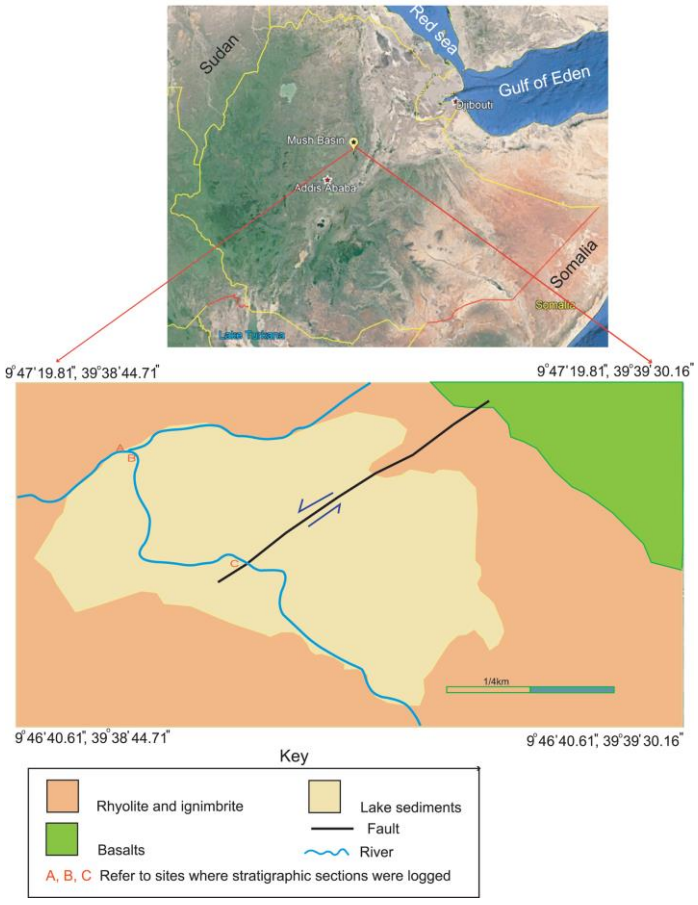

Figure 1. Location map of the Mush Basin in north central Ethiopia and the geological map of the area.

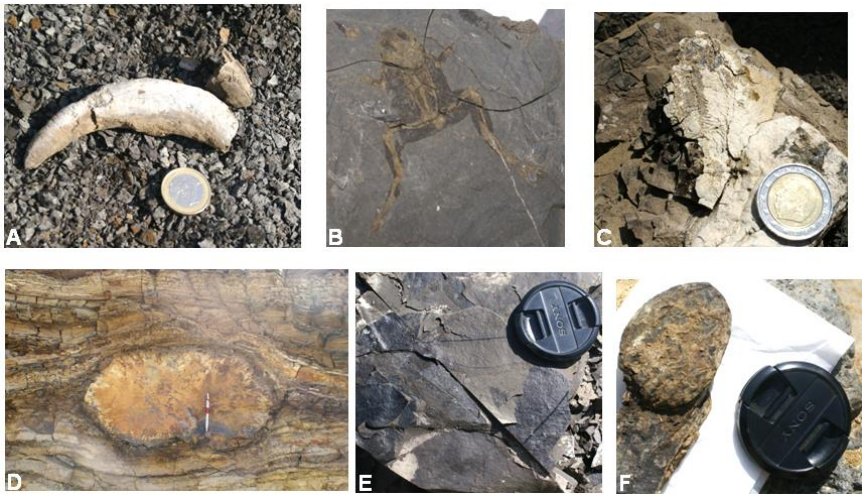

Figure 2. 22 million years-old fossils of: a) pig task, b) frog, c) fish, d) tree log, e) plant leaves and f) seed: from Mush valley, north-central Ethiopia.

Eleven samples given the following field numbers, Mu-1, Mu-3, Mu-4, Mu-5, Mu-7, Mu-10, Mu-11, Mu-12, Mu-13, Mu-14, and Mu-16 were collected for petrographic analysis and twenty two samples were collected for XRD analysis to help interpret the paleoenvironment of the Mush sedimentary basin.

Petrographic analysis was done at the Geological Survey of Ethiopia, Geosciences Laboratory Center; radiometric dating was done in Boise State University Isotope Geology Laboratory, USA; XRD analysis was done at Southern Methodist University, Roy M. Huffington Department of Earth Sciences, Texas, USA; and sedimentary basin delineation and location of sites was done using GPS.

RESULTS

Geological results

The fossil-bearing sedimentary units of the Mush basin are exposed in an area of approximately 4.5 km by 1 km area and the maximum exposed sediment thickness is 55 m (Fig. 3).

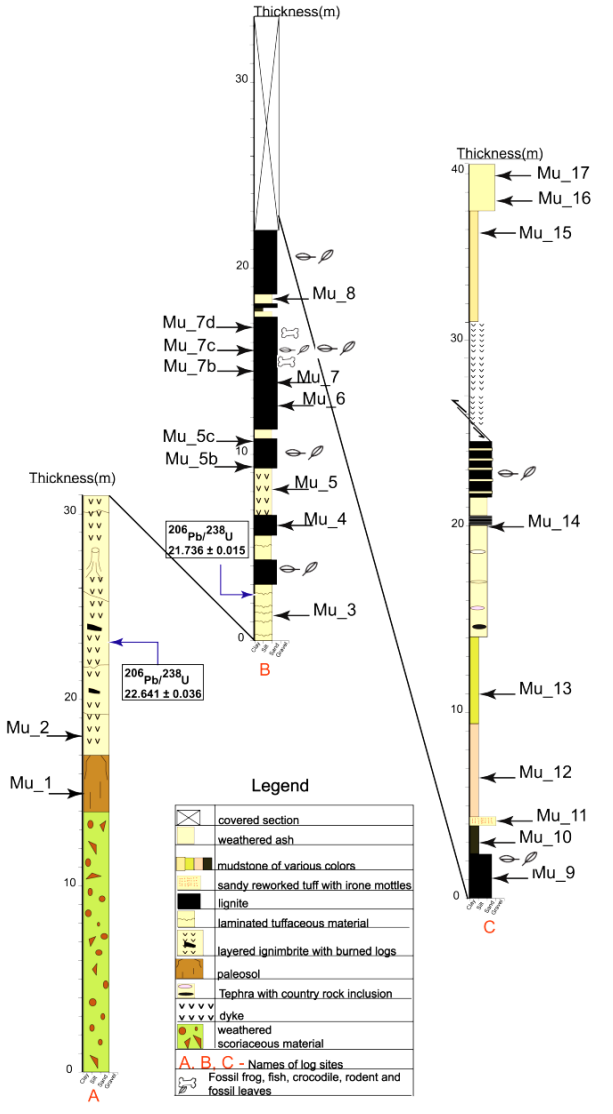

Figure 3. Stratigraphic section of the Mush basin sediments; labels of letters and numbers show locations of sample sites taken for radiometric, petrographic and XRD analyses.

Field traverses around the Mush basin and nearby tributaries resulted in the mapping of the following rock units from lowermost to uppermost: strongly weathered, dark grey, commonly aphanitic to locally phyric scoraceous basalt; paleosol horizon; massive thick ignimbrite and tuffaceous succession; weathered ash-rich carbonaceous sediments; layered ignimbrite unit, carbonaceous shale-rich sediments; mudstone and volcanic ashes; ignimbrite-rhyolite unit and a capping olivine-plagioclase phyric basalt. The previous research by Yonas Hagereselam and Matebie Meten (2006) has demonstrated that the Mush sediments are laid between the lower basalt and the rhyolite-ignimbrite (where we now see a paleosol, thick and massive ignimbrite and tuffaceous succession; weathered ash rich carbonaceous sediments; layered ignimbrite unit, carbonaceous shale rich sediments; mudstone and volcanic ashes) and between the rhyolite-ignimbritic units and upper basalt (where there are weathered ignimbrites). But the field survey conducted in this research has confirmed that the sediments are between the lower welded ignimbrite and layered ignimbrite and the layered ignimbrite and ignimbrite-rhyolite succession (Fig. 3).

Description of the sediments of the Mush basin

Reworked volcaniclastic sediments, lignites, mud units, and carbonaceous shale are the major lithologic units observed (Fig. 4) and the detailed description is provided below.

Reworked volcaniclastic sediments

These units are poor to medium sorted, silty to sand size with angular to sub-rounded reworked pyroclastic and volcanic ash fragments (indicated by red arrow in Fig. 4). Many of the ash units have abundant black colored carbonized wood materials. The color of the units ranges from whitish to yellowish brown to pale gray. The common structures observed include horizontal bedding but mostly massive. In most cases unweathered volcanic glass shards are common but at other instances stains of iron oxide and some iron-mottled structures are very common.

Lignite and carbonaceous shale

Associations of horizontally layered and fissile lenticular lignite seams and carbonaceous shales are very common in the Mush basin sediments (indicated by green arrow in Fig. 4). The carbonaceous shale unit is exceptionally rich in leaf prints, fossil plants including leaves, seeds and various wood parts; and also in fossil animals

including fish, frogs and various mammal fossils. The lignite units are laminated and easily fractured. The color of this unit ranges from dark brown, dark gray to dark.

Mud units

These are fine grained, homogeneous and massive units and lack any recognizable sedimentary structures (indicated by yellow arrow in Fig. 4). The color ranges from buff to dark yellowish gray to brown.

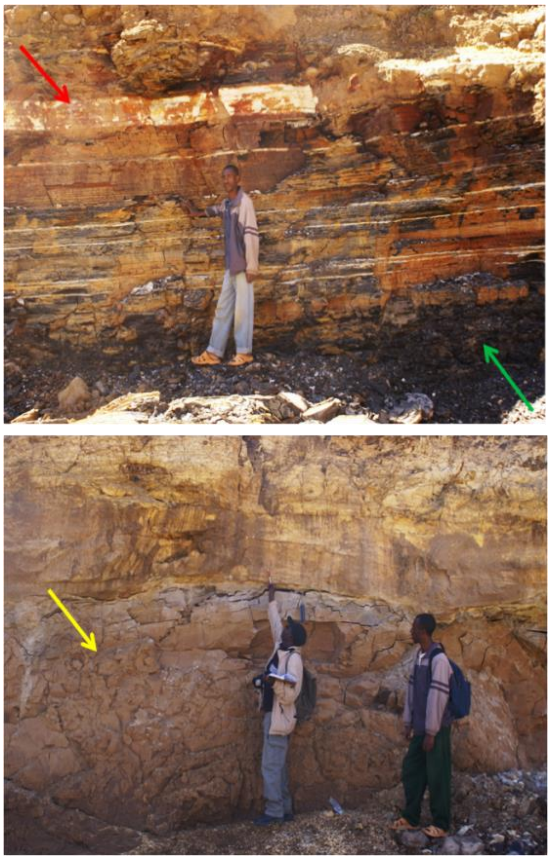

Figure 4. Typical section in the Mush basin with layers ofreworked volcanic ash (marked with red arrow), carbonaceous shale and lignite units (marked with green arrow) and mud unites (marked with yellow arrow).

Results of petrographic analysis

Samples were cut and sliced at the Geological Survey of Ethiopia: Geosciences Laboratory Center. The petrographic analyses showed the following: volcanic glass, quartz, volcanic rock fragment, clay, Most of the identified minerals are primary minerals but volcanic rock fragments, clay, Fe-oxide and devitrified volcanic glass indicate that they are products of weathering of volcanic rock and volcanic ash (Fig. 5).

Results of x-ray diffraction analysis

In many instances, lake sediments are fine-grained and are very hard to analyze using petrographic microscopes alone. Thus, it is important to carry out x-ray diffraction analysis to interpret the depositional environment of the sediments. 22 samples were powdered and analyzed in the XRD laboratory at Southern Methodist University, Texas, USA [Annex II]. Samples analyzed from the paleosol horizon in the lower part of the section (Mu-1) show the presence of lizardite, clintonite and alunogen minerals which are alterations of pyroxene or olivine, mica and hydrated aluminum sulfate clay minerals, respectively. These results indicate the paleosol is derived from the basal basalt at the bottom part of the section. Analyses of Mu-2 and Mu-3 show that the majority of the constituents are primary plagioclase feldspar and reworked ash. Analysis of sample Mu-4 from the lignite bed has resulted in the identification of halloysite clay mineral which is a kaolin mineral family. Analysis of sample Mu-5 identifies anorthite and microcline feldspar minerals, which are distinctively primary minerals. Analyses of samples Mu-5b, Mu-5c, Mu-6, Mu-7, Mu-7b, Mu-7c, Mu-7d, Mu-8, Mu-9, Mu-10, Mu-11, Mu-12, Mu-13, Mu-14 and Mu-15 identified various clay minerals including dickite, clintonite, donpeacorite, norrishite, tobelite, illite and kaolinite.

All of these minerals indicate the formation of mixed-layer clay minerals resulting from the weathering of precursor ferromagnesian minerals and silicates in humid conditions. In contrast, analyses of samples from the top part of the section (Mu-16 and Mu-17) documents the presence of microcline, muscovite and anorthoclase minerals, all of which are primary, demonstrating an abrupt change in depositional environment from clay rich sub-aqueous to sub-areal conditions rich in unaltered tuffs rich in primary sodium feldspar, micas and feldspars minerals.

Radiometric dating

The Mush section has more than 30 meters of tuffacious material, paleosols and layered ignimbrites at the base which are overlain by at least 55 m of lacustrine sediments. $^{206}Pb/^{238}U$ age dating from Zircon was used to date the ignimbrite unit at the base of the sediment section, the Mush sediments and the volcanic ash at the basin wall. $^{206}Pb/^{238}U$ age of the ignimbrite (MV18/Ignimbrite in Annex III) at the base of the section has yielded 22.641 ± 0.036 Ma and provides a maximum age for the section (Fig. 6 and Annex III).

Similarly, $^{206}Pb/^{238}U$ age of the reworked ash (MV8/sed in Annex III) within the Mush sediment succession has yielded 21.736 ± 0.015 Ma. These two ages provide the age of the ignimbrite which underlies the sediment and the age of the sediment succession respectively. Volcanic ash sample was also collected from the ignimbrite succession at the valley wall. This sample from the volcanic succession (M9/wall ash in Annex III) that presumably erupted after the oldest ignimbrite layer in the Mush basin but before the collapse of the volcanic caldera has yielded a $^{206}Pb/^{238}U$ age of 22.309 ± 0.02 Ma (Fig.6 and Annex III).

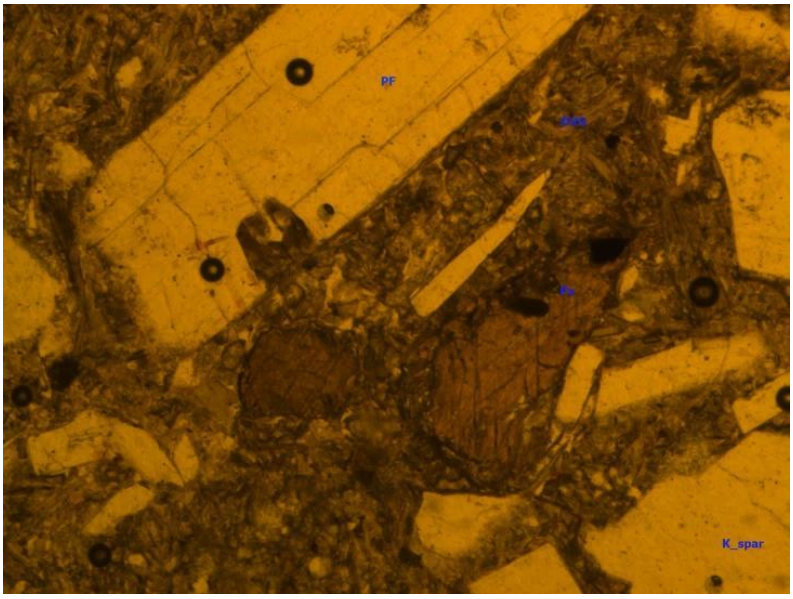

Figure 5. Photomicrograph of claystone (MU3) (at 1.5 meter in stratigraphic Section-B in Figure 3), in plain polarize light at 4x magnification. This shows Plagioclase feldspar (PF), Sanidine -Potassium feldspar (K-spar), Pryroxene (Px) and devitrified volcanic glass (DVG). The ground mass is weathered volcanic ash.

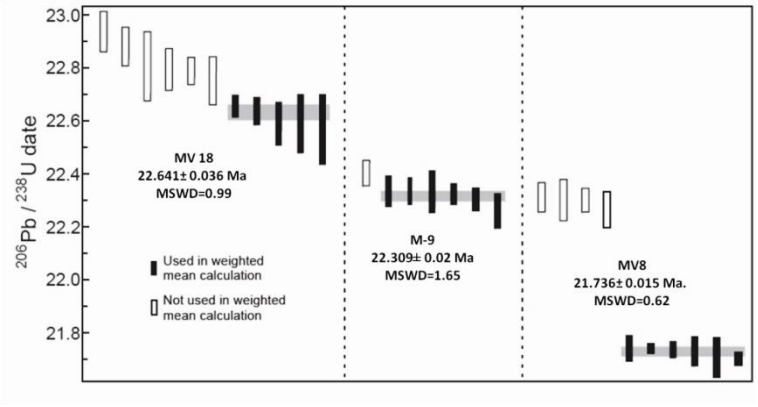

Figure 6.$^{206}Pb/^{238}U$ age dates of three samples: Ignimbrite bed at the base of the Mush sediment succession (MV18), volcanic ash from the volcanic succession of the Mush basin wall (M-9), and a reworked ash from the sediment succession of the Mush basin (MV8).

Interpretation

The field survey and GPS-based delineation of the Mush depositional basin, petrographic analyses, XRD analyses and radiometric dating of key horizons results in a comprehensive understanding of the local geology, environments of deposition, and implications for paleoclimate. The presence of dropped pyroclastic bombs, *in situ* burned woods (Fig. 7), and coarse-grained pyroclastics indicate the presence of a volcanic eruption center close to the Mush basin at the time of sedimentary deposition. The researcher hypothesizes the formation of a volcanic caldera and subsequent caldera-lake in which Mush basin fossiliferous sediments accumulated. The $^{206}Pb/^{238}U$ age of 22.641± 0.036 Ma from the lowest part of the ignimbrite beds near the base of the section dates the likely beginning of eruptive activity intruding through the Alaji Molale basalt (the basalt at the base of the Mush section). The $^{206}Pb/^{238}U$ age of 22.309± 0.02Ma from the ignimbrite-rhyolite from the Mush basin wall provides a date for the formation of a wall-forming ash before the caldera collapsed to form a basin.

Similarly, the $^{206}Pb/^{238}$ U age of 21.736± 0.015 Ma from the ash bed near the base of the sedimentary sequence marks the beginning of post-caldera collapse and accumulation of crater-lake sediments. XRD analyses, which documented the presence of kaolinite, dickite, halloysite and other mixed clays from this part of the sedimentary sequence, provide evidence of a wet climate. The presence of coals, alternating with carbonaceous shales and mudstones, and the presence of fossil frogs and fish (Fig. 8) are consistent with lake-environment and lacustrine sedimentation. The presence of another thick ignimbrite layer overlying the first cycle of sediments in the Mush bottom succession indicates the presence of a second cycle of ignimbrite eruption which was followed by the second cycle of sediment formation. The presence of multiples of NNE-SSW trending faults that cut the Mush sediments and the youngest capping basalt (Tarmaber basalt) indicates the presence of active tectonic process in the region. The XRD identification of microcline, muscovite and anorthoclase-rich thick ash horizons at the top of the Mush sequence indicates an abrupt change in depositional environment from clay-rich lacustrine sedimentation to subaerial conditions.

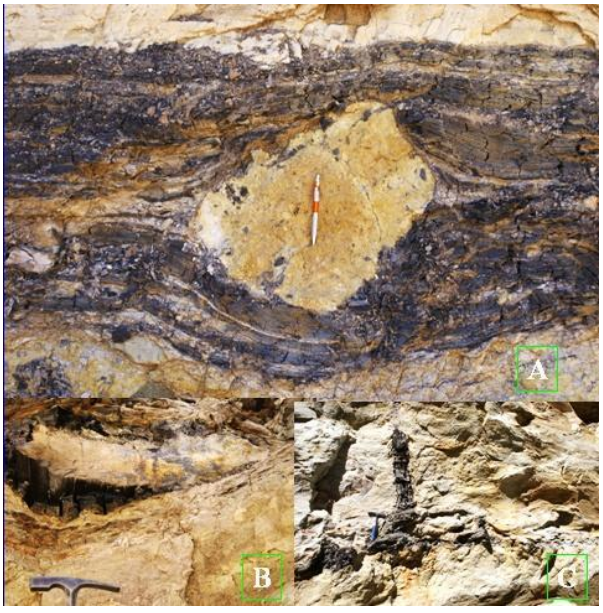

Figure 7.(A) Pyroclastic bomb dropped in a wet lignite bed, burned *in situ* woods (B and C) all indicating the presence of nearby volcanic center in the Mush basin evolution.

Figure 8. Fossil frog (A and C) and fossil fish (B) all indicating fresh water environment of the Mush basin sedimentary environment.

DISCUSSION

Lakes in volcanic provinces can be created in various ways. They can be formed in fault-bounded settings, volcanic calderas and craters or a combination of these settings. To interpret the origin of the Mush basin, intense field surveys were carried out and the following observations were made: a) more than 17 m thick ignimbrite units which host more than a meter thick *in situ* burned tree logs; b) half meter size dropped pyroclastic bombs placed within lignite beds and coarse-grained pyroclastics; c) circular basin morphology and d) absence of fault structures formed before and during sedimentation. A combined interpretation of these features indicates the presence of a volcanic caldera and subsequent caldera-lake in which Mush basin fossiliferous sediments accumulated. Moreover, the presence of another thick ignimbrite layer overlying the first cycle of sediments in the Mush bottom succession indicates the presence of a second cycle of ignimbrite eruption which was followed by the second cycle of sediment formation. Additionally, the presence of about half meter thick pyroclastic bombs dropped into the lignite beds during their active deposition indicates the presence of a volcanic eruption center close to the Mush basin which was erupting at the time of the lignite formation.

The age of the Mush basin sediments was dated to be 21.736 ± 0.015 Ma and this was one of the global warming picks in geological history (Zachos *et al*., 2001). The presence of well-preserved plant leaves in this sedimentary succession has immense contribution to reconstruct the ancient climate and the response of the plants to global warming. The data from Mush has very important information about the plants, CO_2 concentration and the temperature of the time to support the current efforts of climate modeling and understanding global warming phenomena (Tekie Tesfamichael *et al* 2017). XRD analyses of the Mush sediments have indicated the presence of kaolinite, dickite, halloysite and other mixed clays which provide evidence of a wet climate. The presence of coals, alternating with carbonaceous shales and mudstones, and the presence of fossil frogs and fish is also consistent with lake-environment and lacustrine sedimentation. A similar interpretation was made by Jon and Daphne (2009) where excellent fish and plant preservation in anoxic conditions was considered as indicator for lake sedimentation.

However, analyses of samples from the top part of the Mush sequence documents the presence of microcline, muscovite and anorthoclase minerals, all of which are primary. The XRD identification of these minerals at the top of the section indicates an abrupt change in depositional environment from clay-rich lacustrine sedimentation to subaerial conditions, promoting deposition of unaltered volcanic ashes. This is supported by the presence of multiple NNE-SSW trending faults that cut the top-most section of the Mush sediments and the youngest capping basalt (Tarmaber basalt) which indicates the presence of active tectonics and faulting in the region at the later time of the basin evolution. Looking at the sudden relationship between the organic-rich lake sediments and unaltered thick ash horizons indicates a faulting event which might have caused the final drying up of the Mush Lake.

CONCLUSIONS

The Mush basin, located in the central plateau of north-central Ethiopia is situated in a volcanic province and is filled by successions of Tertiary volcanics and interbeded sedimentary sequences. Research in the basin has yielded in the discovery of unique floral and faunal assemblages, with significant potential for paleoclimate reconstructions and new data on the geological history of the Ethiopian Highlands.

Detailed field survey, petrographic and XRD analyses, and radio-isotopic age determinations were used to understand the origin, age, geological history and environment of the sedimentary basin and to provide a physical setting to understand the ancient flora, fauna, and climate of the area. The geology of the Mush basin constitutes a basal scoraceous basalt, followed by deposits that include: paleosols, ignimbrites, tuffaceous beds, lacustrine carbonaceous shales, mudstones, and sandstones capped by extensive beds of rhyolite, ignimbrite and porphyritic basalt. The lacustrine carbonaceous shales (intercalated with lignitic strata and periodic ash beds) host abundant compressions of leaves, fruits, seeds, insects, pollen, woods, concentrations of organically preserved amphibians as well as infrequent remains of crocodiles and mammals. Fieldwork also identified nearby multiple volcanic episodes, some of which are associated with volcanic bombs (emplaced in the lignite beds) of up to a meter in diameter, and several in situ carbonized trees.

Results of petrographic analyses from throughout the section indicate the presence of primary minerals like plagioclase feldspar, potassium feldspar and pryroxene; whereas XRD analyses of several samples document the presence of clay minerals: kaolinite and illite.

The origin of the Mush basin is interpreted as volcanic caldera, but several NNE-SSW trending faults associated withthe Main Ethiopian Rift System have severely affected the sediments after deposition. The age of the Mush lacustrine sediments is determined from $^{206}Pb/^{238}U$ radio isotopic dating of a volcanic ash in the lower layer of the fossiliferous carbonaceous shale, indicating the early stage of lacustrine deposition at 21.736 ± 0.015 Ma.

X-ray diffraction analyses and the study of field relationships indicate that the fossiliferous shales were formed in a volcanic caldera and originated in a fresh water lake. These conclusions are consistent with the presence of organically-preserved amphibians and aquatic plants, and indicate a climate having abundant precipitation.

ACKNOWLEDGEMENTS

This research was conducted through fund supported by Addis Ababa University, the National Science Foundation and the National Geographic Society. Thanks go to Prof. Bonnie Jacobs, Prof. Louis Jacobs, Prof. Neil Tabor, Dr. Ellen Currano, Dr. Tekie Tesfamichael, and Dr. Aaron Pan for their valuable inputs for this research. I thank the Authority for Research and Conservation of Cultural Heritage of the Ministry of Culture and Tourism and the North Shoa zonal administration and culture and tourism offices, Ethiopia, for giving us the permit to work in the site and for their boundless support during the times of the research. The author would also like to thank Dr. Scott Myers from Department of Geological Sciences, Southern Methodist University, for his support during the XRD analysis. Thanks also go to the Mush basin community for their support and cooperation.

REFERENCES

1. Alula Habtegiorgis and Gashawbeza Mengstu (1993). Report on the coal occurrence of Mush Valley, Ethiopian Institute of Geological Surveys (Unpub. Rep.), Addis Ababa Ethiopia, 19 pp.
2. Berberi, F., Borsi, S., Ferrara, G., Marinelli, G., Santacroce. R., Tazieff, H., and Varet, J. (1972). Evolution of the Danakil Depression (Afar, Ethiopia) in light of radiometric age determinations. *Journal of Geology* **80**: 720-729.
3. Burke, K. and Dewey, J. K. (1973). Plume generated triple junctions: Key indications in applying plate tectonics to old rocks. *Journal of Geology*, **81**: 406-433.
4. Clemens, M. (2014). 22 million year-old frogs from the Miocene of Mush, Ethiopia. Unpublished MSc. Thesis, Roy M. Huffington Department of Earth Sciences, Southern Methodist University, Dallas, Texas, U.S.A, 54pp.
5. Currano, E.D., Jacobs, B.F., Pan, A.D., and Tabor, N.J. (2011). Inferring ecological disturbance in the fossil record: a case study from the late Oligocene of Ethiopia. *Palaeogeography, Palaeoclimatology, Palaeoecology* **309**(3): 242–252.
6. Dereje Ayalew (2011). The relations between felsic and mafic volcanic rocks in continental flood basalts of Ethiopia: implication for the thermal weakening of the crust, *Geological Society of London Special Public*ations, **357**(1): 253-264.
7. Dereje Ayalew, Barbey, P., Marty, B., Reisberg, L., Gezahegh Yirgu and Pik, R. (2002). Source, genesis, and timing of giant ignimbrite deposits

associated with Ethiopian continental flood basalts. *Geochimica et Cosmochimica Acta*, **66** (8): 1429–1448.

8. Engel, M., Pan, A.D. and Jacobs, B.F. (2013). A termite from the Late Oligocene of northern Ethiopia.*ActaPalaeontologicaPolonica*.**58**: 331–334.
9. Gashawbeza Mengistu, and Mesfin Wubshet (1996). Report on Geological and Geophysical Exploration for Coal Occurrence at Mush Valley, Ethiopian Institute of Geological Surveys, (Unpub. Rep.), Addis Ababa Ethiopia, 37pp.
10. Massini, G., J.L., Jacobs, B. F., Pan, A., Tabor, N., Kappelman, J. (2006). The occurrence of the fern *Acrostichum* in Oligocene volcanic strata of the northwestern Ethiopian plateau. *International Journal of Plant Sciences*,**167**: 909-918.
11. Massini, G., J.L., Jacobs, B., and Tabor, N. (2010). Paleoenvironmental reconstruction of Late Oligocene terrestrial volcaniclastic deposits from the northwestern Ethiopian Plateau. *Palaeontologia Electronica* **13**(1): 13.1.6A.
12. Jacobs, B. F. (2007). Fossils from ancient forests in Africa provide a palaeobotanist with insight into past climates. *Nature Journal Club* **447:** 119.
13. Jacobs, B.F., Pan, A.D., and Scotese, C. (2010). A review of the Cenozoic vegetation history of Africa. In: (Werdelin, L. and Sanders, W., eds.), *Cenozoic Mammals of Africa*. University of California Press, 72pp.
14. James M. Mattinson (2005). Zircon U–Pb chemical abrasion ("CA-TIMS") method: Combined annealing and multi-step partial dissolution analysis for improved precision and accuracy of zircon ages, *Chemical Geology*, **220**(1–2): 47-66.
15. Jaffey, A.H., K.F. Flynn, L.E. Glendenin, W.C. and Bentley, A.M. (1971). Essling Precision measurement of half-lives and specific activities of ^{235}U and ^{238}U, *Physics Reviews*, **4**: 1889-1906.
16. Lindqvist, Jon K. and Daphine E (2009). High-frequency paleoclimate signals from Foulden Maar, Waipiata Volcanic Field, southern New Zealand: An Early Miocene varved lacustrine diatomite deposit. *Sedimentary Geology*, **222**, (Issues 1–2): 98-110.
17. Kappelman, J., Rasmussen, D.T., Sanders, W.J., Mulugeta Feseha, Bown, T., Copeland, P., Crabaugh, J., Fleagle, J., Glantz, M., Gordon, A., Jacobs, B., Maga, M., Muldoon, K., Pan, A., Pyne, L., Richmond, B., Ryan, T., Seiffert, E.R., Sen, S., Todd, L., Wiemann, M.C., and Winkler, A. (2003). Oligocene mammals from Ethiopia and faunal exchange between Afro-Arabia and Eurasia, *Nature*, **426**: 549-552.
18. Kieffer, B., Arndt, N., Lapierre, H., Bastien, F., Bosch, D., Pecher, A., Gezahegn Yirgu, Dereje Ayalew, Weis, D., Jerram, D.A., Keller, F., and Meugniot, C. (2004). Flood and shield basalts from Ethiopia: magmas from the African super swell. *Journal of Petrology*, **45** (4): 793–834.
19. Schmitz, M. D. and Schoene, B. (2007). Derivation of isotope ratios, errors, and error correlations for U-Pb geochronology using ^{205}Pb-^{235}U-(^{233}U)-spiked isotope dilution thermal ionization mass spectrometric data, *Geochemistry, Geophysics Geosystems*, **8**(8): 1-20.
20. Mohr, P. A. (1983). The Ethiopian flood basalt province. *Nature,* **303**: 577-584.
21. Mohr, P.A. (1971). Ethiopian Rift and Plateaus: Some Volcanic Petrochemical Differences. *Journal of Geophysical Research*, **76**: 1967-1984.
22. Mulugeta Feseha, Dereje Ayalew, Kassaye Begashaw and Solomon Yirga (2008). Paleoenvironmental reconstruction of ancient lakes and exploration of associated economic minerals and fossils: Project Report, Addis Ababa University, Addis Ababa, Ethiopia, 41 pp.
23. Mulugeta Feseha (2005). Sequence stratigraphic interpretation of the Chilga basin sediments, northwest Ethiopia. *SINET: Ethiopian Journal of Science,* **28** (1): 75-92.
24. Mulugeta Feseha (2002). Sequence Stratigraphy, Petrography and Geochronology of Continental Rift Basin Sediments, Chilga area, Northwest Ethiopia, Dissertation, University of Texas at Austin, 330pp.
25. Mulugeta Feseha, Kocurek, G., Kappelman, J.and Copeland, P. (2001). Sequence Stratigraphy, Petrography and Geochronology of the Oligocene Chilga Rift Basin Sediments, Northwest Ethiopia. *AAPG Annual Convention*, June 3-6, Denver, CO, Abstract with Programs.
26. Pan, A.D., Currano, E.D., Jacobs, B.F., Mulugeta Feseha, Tabor, N.J., and Herendeen P. S. (2012). Fossil Newtonia (*Fabaceae: Mimoseae*) Seeds from the Early Miocene (22–21 Ma) Mush Valley in Ethiopia, *International Journal of Plant Sciences*, **173**(3).
27. Pan, A. D. (2010). Rutaceae leaf fossils from the Late Oligocene (27.23 Ma) Guang River flora of northwestern Ethiopia. *Review of Palaeobotany and Palynology,* **159**: 188-194.
28. Pan, A. D., Jacobs, B.F., Herendeen (2010). P. Detarieaesensulato (*Fabaceae*) from the Late Oligocene (27.23 Ma) Guang River flora of north-western Ethiopia. *Botanical Journal of the Linnean Society,* **163**: 44 – 54.
29. Pan, A. (2007). The late Oligocene (28-27 Ma) Guang River flora from the northwestern Plateau of Ethiopia: PhD dissertation, Southern Methodist University, Dallas, TX, 235pp.
30. Pan, A.D., Jacobs, B.F., Dransfield, J., and Baker, W.J. (2006). The fossil history of palms (*Arecaceae*) in Africa and new records from the Late Oligocene

(28-27 Ma) of north-western Ethiopia. *Botanical Journal of the Linnean Society*, **151**: 69-81.

31. Stacey, J.S. and Kramers, J.D. (1975). Approximation of Terrestrial Lead Isotope Evolution by a 2-Stage Model. *Earth and Planetary Science Letters,* **26**(2): 207-221.
32. Tesfamichael Tekie, Jacobs, B., Tabor, N., Michel, L., Currano, E., Mulugeta Feseha, Barclay, R., Kappelman, J. and Schmitz, M. (2017). Settling the issue of "decoupling" between atmospheric carbon dioxide and global temperature: [CO2]atm, reconstructions across the warming Paleogene-Neogene divide. *Geological Society of America*, DOI:10.1130/G39048.1
33. Yonas Hagereselam and Matebie Meten (2006). Report on Geology of the Sela Dingay (C) and Debreberhan (J) Sub-sheets of Debreberhan Map Sheet (NC 37-11), Geological Survey of Ethiopia, Regional Geology and Geochemistry Department, Ministry of Mines and Energy (Unpub. Rep.), Addis Ababa Ethiopia, 51 pp.
34. Zachos, J., Pagni, M., Sloan, L., Thomas, E., and Billups, K. (2001). Trends, rhythms, and aberrations in global climate 65 Ma to present, *Science*, **292:** 686-693.

Annex I. Sample data of petrographic analysis

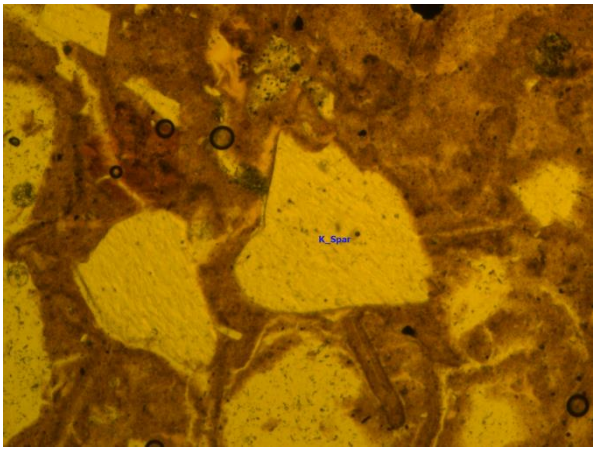

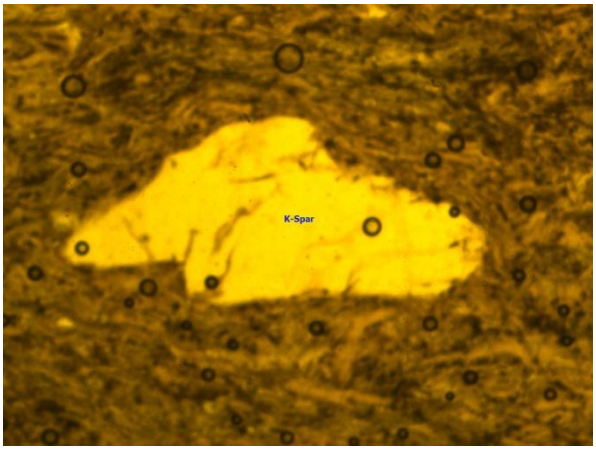

Photomicrograph of reworked ash (MU1) in plain polarized light, at 15 meters in stratigraphic Section_1 in Figure 3 (left). This photo shows abundant Potassium feldspar (K-spar) and reworked volcanic ash as groundmass. On the right side shows MU9 with organic matter as ground mass and few Potassium feldspar (sanidine) grains. MU9 is sampled at 1m in Section_3 of Figure 3.

Annex II. Sample data of x-ray diffraction analysis results of Mush sediments. Analysis was carried out at Southern Methodist University, Dallas, Texas, USA.

No	Sample name	Lithology	Identified minerals by XRD	Chemical Formula	Mineral nature	Environmental interpretation
1	MU17	Whitish mottled weathered tuff	Anorthoclase	(Na,K)(Si3Al)O8	Primary	Sodium feldspar
2	MU16	whitish weathered tuff	Microcline and Muscovite-2M1 and Anorthoclase	KAlSi3O8 and KAl2(Si3Al)O10(OH,F)2 and (Na,K)(Si3Al)O8	Microcline and Muscovite-2M1 and Anorthoclase -all seem rock-forming minerals. Microcline is an intrusive equivalent of Anorthoclase. Muscovite-2M1 is a high temperature phase resulted from transformation. Both primary minerals	Micas and feldspars
3	MU15	varigated color weathered tuff	Kernite and Dickite-2M1 and Saponite-15A	Na2B4O6(OH)2.3H2O and Al2Si2O5(OH)4 and (Mg2Al)(Si3Al)O10(OH)2.4H2O	Secondary	hydrated sodium borate hydroxide mineral and kaolin group clay mineral and smectite clay resulted from weathering of tuff

4	MU14	whitish weathered tuff/clay	Stevensite-15A and Alunogen and Anatase	Ca0.2Mg2.9Si4O10(OH)2.4H2O and Al2(SO4)3·17H2O and TiO2	Secondary	smectite group of clay minerals and hydrated aluminium sulfate, clay mineral and oxide of titanium
5	MU13	Calystone (greenish clay)	Schoderite and Alunogen and Anatase	Al2(PO4)(VO4)8(H2O)and Al2(SO4)3·17H2O and TiO2	Secondary	Vanadium mineral and hydrated aluminium sulfate, clay mineral and oxide of titanium
6	Mu12	Claystone (brownish color)	Quartz and Sweetite	SiO2 and Zn(OH)2	Quartz is primary, but Sweetite is secondary	silica and zinc oxides forming clay mineral
7	MU11	motteled weathered ash	Baratovite and Alunogen and Sanidine	KCa7(Ti,Zr)2Li3Si12O36F2 and Al2(SO4)3.17H2O and K(Si3Al)O8	Baratovite and Alunogen are secondary, but Sanidine is primary	Silicates mineral and hydrated aluminium sulfate, clay mineral and potassium feldspar
8	MU10	Claystone (greenish color)	Saponite-15A, Schoderite and Anatase	(Mg2Al)(Si3Al)O10(OH)2.4H2O and Al2(PO4)(VO4)8(H2O) and TiO2	Secondary	smectite clay resulted from weathering of tuff, vanadium mineral and oxide of titanium
9	MU9	Lignite	Chromium	CR	Cr is an element; it can occur in high concentration if the Lignite is formed in basaltic environment	Cr bearing organic matter
10	MU8	Volcanic ash (reworked)	Alunogen	Al2(SO4)3·17H2O	Secondary	Hydrated aluminium sulfate, clay mineral
No	Sample name	Lithology	Identified minerals by XRD	Chemical Formula	Mineral nature	Environmental interpretation
11	MU7D	Lignite	Anatase and illite	TiO2 and KAl2(Si3Al)O10(OH)2	Secondary	Oxide of titanium and potassic clay mineral which can be formed through the weathering of muscovite, not well drained potassium, when no potassium becomes smectite
12	MU7C	Lignite	illite	KAl2(Si3Al)O10(OH)2 and	Secondary	potassic clay mineral which can be formed through the weathering of muscovite, when there is potassium, when no potassium becomes smectite

13	MU7B	Lignite	Clintonite-1M and Tobelite-1M	Ca(Mg,Al,Fe)3(Al,Si)4O10(OH)2 and NH4Al2(Si3Al)O10(OH)2	Secondary	Altered mica to clay
14	MU7	Lignite	Hydroxylapatite and Fluorapatite	Ca5(PO4)3(OH) and Ca5(PO4)3F	Primary	primary calcium and phosphate mineral
15	MU6	Lignite	Donpeacorite and Norrishite	MgMnSi2O6 and KMn3+2LiSi4O12	Both are secondary	Clay mineral alterations of orthopyroxene and mica
16	MU5C	Lignite	Clintonite-1M and Orthoclase	Ca(Mg,Al,Fe)3(Al,Si)4O10(OH)2 and KAlSi3O8	Clintonite-1M is secondary while Orthoclase is primary	Clay and feldspar
17	MU5B	Lignite	Anatase and Dickite-2M1	TiO2 and Al2Si2O5(OH)4	Both are secondary	naturally occurring oxide of titanium and kaolin group clay mineral
18	MU5	Claystone (reworked ash)	Anorthie and Microcline	(Ca,Na)(Al,Si)2Si2O8 and KAlSi3O8	Primary	Feldspar groups
19	Mu4	Lignite	Halloysite-7A	Al2Si2O5(OH)4	Secondary	Clay mineral like Kaolin
20	MU3	Claystone (reworked ash)	Anorthite	(Ca,Na)(Al,Si)2Si2O8	primary	Plagioclase Feldspar
21	MU2	silty size volcanic ash (ashy color)	Quartz, Zinc bis(hydroxyanthrapyrimidine) dihydrate	SiO2 and C30H14N4O4Zn.2H2O	Quartz - primary, Zinc bisdihydrate is secondary	Altered ash into clay
22	MU1	paleosol gray clay	lizardite and clintonite and Alunogen	Mg3Si2O5(OH)4 and Ca(Mg,Al,Fe)3(Al,Si)4O10(OH)2 and Al2(SO4)3·17H2O	Secondary minerals formed by alterations	Alterations of pyroxene or olivine and mica and hydrated aluminum sulfate clay mineral

Annex III .Table showing U-Pb results.

U-Th-Pb isotopic data

	Compositional Parameters						Radiogenic Isotope Ratios								Isotopic Ages			
Sample	Th/U	$^{206}Pb^*$ x10^{-13}mol	mol % $^{206}Pb^*$	Pb^*/Pb_c	Pb_c (pg)	$^{206}Pb/^{204}Pb$	$^{208}Pb/^{206}Pb$	$^{207}Pb/^{206}Pb$	% err	$^{207}Pb/^{235}U$	% err	$^{206}Pb/^{238}U$	% err	corr. coef.	$^{207}Pb/^{235}U$	±	$^{206}Pb/^{238}U$	±
(a)	(b)	(c)	(c)	(c)	(c)	(d)	(e)	(e)	(f)	(e)	(f)	(e)	(f)		(g)	(f)	(g)	(f)
MV8/Sed																		
z12	0.759	0.1249	0.871	2.2	1.52	143	0.245	0.04690	1.8	0.022431	1.9	0.003469	0.205	0.658	22.52	0.42	22.323	0.046
z9	0.655	0.0804	0.830	1.5	1.36	108	0.211	0.04690	2.8	0.022425	3.0	0.003468	0.283	0.680	22.52	0.66	22.315	0.063
z3	0.693	0.0821	0.892	2.6	0.82	168	0.223	0.04676	2.7	0.022346	2.8	0.003466	0.238	0.734	22.44	0.63	22.306	0.053
z8	0.607	0.0892	0.944	5.2	0.44	321	0.196	0.04514	2.5	0.021520	2.6	0.003457	0.326	0.422	21.62	0.55	22.249	0.072
z14	0.742	0.1007	0.884	2.5	1.09	158	0.239	0.04730	2.2	0.022050	2.3	0.003381	0.220	0.722	22.15	0.51	21.758	0.048
z13	0.685	0.1216	0.939	4.8	0.66	294	0.221	0.04577	1.7	0.021321	1.8	0.003379	0.187	0.687	21.42	0.39	21.745	0.041
z10	0.804	0.0812	0.866	2.1	1.04	137	0.259	0.04745	2.6	0.022106	2.8	0.003379	0.253	0.714	22.20	0.61	21.743	0.055
z7	0.663	0.1317	0.971	10.3	0.33	613	0.214	0.04678	0.9	0.021792	1.0	0.003378	0.121	0.667	21.89	0.21	21.741	0.026
z2	0.836	0.2049	0.945	5.7	0.98	332	0.269	0.04639	1.1	0.021588	1.2	0.003375	0.137	0.704	21.69	0.26	21.720	0.030
z11	0.748	0.0860	0.830	1.6	1.45	108	0.241	0.04702	2.7	0.021869	2.9	0.003373	0.273	0.628	21.97	0.63	21.710	0.059

Weighted Mean Date

MV8

$^{206}Pb/^{238}U$ ± random (+tracer) [+l]			MSWD	prob. Fit
21.736	± 0.015 (0.02) [0.03]	± 2s int.	0.62	0.68324
	± 0.015 (0.02) [0.03]	± 95% c.i.*	n =	6

M9/Wall ash

z7	0.678	0.0834	0.894	2.7	0.81	172	0.218	0.04777	2.6	0.022936	2.8	0.003482	0.251	0.721	23.03	0.64	22.408	0.056
z10	0.621	0.1207	0.918	3.5	0.89	221	0.200	0.04661	2.2	0.022304	2.3	0.003471	0.277	0.507	22.40	0.51	22.335	0.062
z2	0.631	0.1837	0.879	2.3	2.09	152	0.203	0.04665	1.6	0.022314	1.7	0.003469	0.183	0.645	22.41	0.39	22.326	0.041
z9	0.591	0.0988	0.916	3.4	0.75	216	0.190	0.04678	2.0	0.022376	2.2	0.003469	0.225	0.701	22.47	0.48	22.325	0.050
z6	0.630	0.1061	0.825	1.5	1.86	105	0.203	0.04683	2.6	0.022400	2.7	0.003469	0.272	0.570	22.49	0.60	22.324	0.061
z8	0.651	0.1423	0.899	2.8	1.32	182	0.210	0.04637	1.6	0.022161	1.7	0.003466	0.175	0.691	22.26	0.37	22.304	0.039
z11	0.632	0.1627	0.848	1.7	2.41	121	0.203	0.04618	1.6	0.022012	1.7	0.003457	0.223	0.511	22.11	0.38	22.248	0.050

Weighted Mean Date

M9

$^{206}Pb/^{238}U$ ± random (+tracer) [+l]			MSWD	prob. Fit
22.309	± 0.02 (0.02) [0.03]	± 2s int.	1.65	0.14268
	± 0.032 (0.03) [0.04]	± 95% c.i.*	n =	6

MV18/Ignimbrite

z8	0.893	0.0513	0.804	1.4	1.04	93		0.287	0.04735	5.1	0.023792	5.4	0.003645	0.418	0.595		23.88	1.26	23.451	0.098

z5	0.716	0.0392	0.840	1.7	0.62	113		0.231	0.04727	5.7	0.023237	5.9	0.003565	0.430	0.615		23.32	1.36	22.940	0.098
z7	1.067	0.0521	0.847	1.9	0.78	118		0.344	0.04726	4.3	0.023194	4.5	0.003560	0.372	0.686		23.28	1.05	22.906	0.085
z12	0.763	0.0414	0.843	1.7	0.64	115		0.246	0.04792	5.5	0.023423	5.7	0.003545	0.434	0.656		23.51	1.33	22.814	0.099
z6	0.735	0.0526	0.896	2.8	0.51	174		0.237	0.04577	3.2	0.022354	3.3	0.003542	0.282	0.679		22.45	0.74	22.792	0.064
z15	0.838	0.0461	0.845	1.8	0.70	117		0.270	0.04958	5.5	0.024201	5.9	0.003540	0.476	0.689		24.28	1.40	22.783	0.108
z14	0.778	0.0199	0.757	1.0	0.53	74		0.251	0.04600	15.2	0.022445	15.5	0.003539	0.729	0.415		22.54	3.45	22.772	0.166
z13	0.869	0.0708	0.891	2.7	0.72	166		0.280	0.04617	3.1	0.022418	3.3	0.003522	0.294	0.705		22.51	0.74	22.664	0.066
z2	0.818	0.0795	0.917	3.6	0.60	217		0.263	0.04719	2.4	0.022915	2.6	0.003522	0.242	0.667		23.01	0.58	22.661	0.055
z10	0.733	0.0300	0.801	1.3	0.62	91		0.236	0.04561	10.7	0.022086	11.0	0.003512	0.605	0.495		22.18	2.41	22.601	0.136
z9	0.753	0.0424	0.861	2.0	0.57	130		0.243	0.04586	8.8	0.022192	9.3	0.003509	0.638	0.755		22.29	2.05	22.582	0.144
z4	0.729	0.0330	0.839	1.6	0.53	112		0.235	0.04206	13.2	0.020339	13.3	0.003507	0.461	0.326		20.44	2.70	22.568	0.104

Weighted Mean Date

MV18

$^{206}Pb/^{238}U$ ± random (+tracer) [+l]			MSWD	prob. Fit
22.641	± 0.036 (0.04) [0.05]	± 2s int.	0.99	0.40932
	± 0.036 (0.04) [0.05]	± 95% c.i.*	n =	5

(a) z1, z2 etc. are labels for single zircon grains or fragments, annealed and chemically abraded after Mattinson (2005); bold indicates grains used in weighted mean calculation.

(b) Model Th/U ratio calculated from radiogenic 208Pb/206Pb ratio and 207Pb/235U age.

(c) Pb* and Pbc represent radiogenic and common Pb, respectively; mol % $^{206}Pb^*$ with respect to radiogenic, blank and initial common Pb.

(d) Measured ratio corrected for spike and fractionation only. Pb isotopic fractionation estimated at 0.18 +/- 0.03 %/a.m.u., based on analysis of NBS-981 and NBS-982.

(e) Corrected for fractionation, spike, and common Pb; up to 0.7 pg of common Pb was assumed to be procedural blank: 206Pb/204Pb = 18.042 ±0.61%; 207Pb/204Pb = 15.537 ± 0.52%; 208Pb/204Pb = 37.686 ± 0.63% (all uncertainties 1-sigma). Excess over blank was assigned to initial common Pb, using the Stacey and Kramers (1975) two-stage Pb isotope evolution model at the nominal sample age.

(f) Errors are 2-sigma, propagated using the algorithms of Schmitz and Schoene (2007).

(g) Calculations are based on the decay constants of Jaffey*et al.* (1971). 206Pb/238U and 207Pb/206Pb ages corrected for initial disequilibrium in 230Th/238U using Th/U [magma] = 3